We E106 14

# Adaptive Waveform Inversion - FWI Without Cycle Skipping - Applications

L. Guasch* (Sub Salt Solutions Ltd) & M. Warner (Imperial College London)

## SUMMARY

Conventional FWI suffers from cycle skipping if the starting model is inadequate at the lowest frequencies present in a dataset. The newly developed technique of adaptive FWI overcomes cycle skipping, and is able to invert normal bandwidth data beginning from an inaccurate velocity model. Here we apply the method to data extracted from a 3D field model, and show that the new method outperforms conventional FWI when starting at higher frequencies than have previously been used to invert this field dataset. We also apply the new methodology to a synthetic dataset that is not cycle skipped, but that is dominated by reflected rather than refracted arrivals. In this case, we show that adaptive FWI also produces a superior result because it has enhanced sensitivity to reflection data, and is able to update the velocity macro-model successfully using reflection-only data.

## Introduction

Conventional full-waveform inversion minimises the least-squares difference between an observed and a predicted dataset. Because seismic data are oscillatory, this formulation leads to an objective function that is also oscillatory, leading to many local minima that represent cycle-skipped solutions where the predicted and observed datasets differ by an integer number of cycles. This behaviour is the principal reason why FWI requires low frequencies and a highly accurate starting model.

In a companion paper (Warner & Guasch, 2014), we presented an adaptive version of FWI, in which Wiener filters are used to match predicted and observed data, and the inversion is formulated so that it forces the filter coefficients to become zero-lag delta functions. In that paper, we demonstrate that this scheme is unaffected by cycle skipping, and is able to recover the global minimum model without low frequencies or a high-quality starting model. In the present paper, we explore the properties this new method, using it to analyse a model from a field dataset, and demonstrating that adaptive FWI is also better able to recover the macro velocity model from reflected energy than is conventional FWI.

## Methodology

Conventional FWI seeks to minimise the least-squares objective function $f$, where

$$f = \| \mathbf{p}(\mathbf{m}) - \mathbf{d} \|^2 \tag{1}$$

where the column vector **d** represents the field data, and **p** represents the equivalent data predicted by a model **m**. In contrast, adaptive FWI employs Wiener filters to match the two datasets, performing the inversion in two stages. The first stage is to design a convolutional filter **w**, that matches a predicted trace **p** to an observed trace **d**, by minimising the least-squares objective function $f_1$, where

$$f_1 = \| \mathbf{P}\mathbf{w} - \mathbf{d} \|^2 \tag{2}$$

where **P** is a matrix representation of convolution by the vector **p**. Then, in a second inversion, we minimise a second normalized least-squares objective function $f_2$, given by

$$f_2 = \frac{\|\mathbf{T}\mathbf{w}\|^2}{\|\mathbf{w}\|^2} \tag{3}$$

where **T** is a simple diagonal matrix that acts to weight the filter coefficients as a function of the magnitude of the temporal lag. Minimising $f_2$ with respect to the model **m** pushes the predicted data **p** towards the observed data **d**, and so pushes the model **m** towards the true model. The objective functions $f_1$ and $f_2$ are not oscillatory and do not suffer from the detrimental effects of cycle skipping.

## Application to a field dataset

We have previously extensively analysed a 3D OBC anisotropic dataset acquired over the shallow-water Tommeliten field in the North Sea. Here we apply both conventional and adaptive FWI to data generated along a 2D slice through this 3D model. We do not yet have a full 3D version of our adaptive method operational in anisotropic models, but the method is readily extendable and affordable in 3D – its only additional costs are the generation of one-dimensional Wiener filters for each data trace at each iteration, together with some other one-dimensional operations on each trace.

In our original 3D field study, we began the inversion at 3 Hz. Although the absolute amplitudes of the raw field data at 3 Hz are about 40 dB below the amplitudes at 10 Hz, we were fortunate in that the signal-to-noise ratios at 3 Hz in this OBC dataset were sufficiently high that we could begin FWI at these low frequencies. However, in many field datasets, and especially in those acquired with surface streamers, such low frequencies are less readily available. In this 2D study therefore, we ran the inversion at 6 Hz, at which frequency we expect conventional FWI to suffer from the detrimental effects of cycle skipping, and where we have the expectation that adaptive FWI will still succeed.

Figure 1(a) shows a 2D slice through the 3D starting model. This starting model was used for both the original 3D field study and in the present 2D study. This model was generated by anisotropic reflection travel-time tomography. The low-velocity feature in the centre of the model is a shallow gas cloud within a clastic section above a deeper, faster chalk reservoir near the base of the model. The detailed geometry and velocity structure of this gas cloud was the principal target of the 3D FWI. Figure 1(b) shows the same 2D slice through the 3D model that we have previously recovered using conventional FWI starting at 3 Hz (Warner *et al.*, 2013). This model produces significant uplift in the PSDM at reservoir depth, and better matches well logs and flattens gathers than does the start model.

Figure 1(c) shows the model that conventional 2D FWI recovers, from data generated along this 2D slice, when the inverted data have a dominant frequency of about 6 Hz. The source wavelet used in the modelling and inversion rolls off rapidly above 6 Hz, and the field data itself rolls off rapidly below 6 Hz. In these 2D time-domain inversions, we did not increase frequency as the inversion proceeded; we inverted all the data at each iteration.

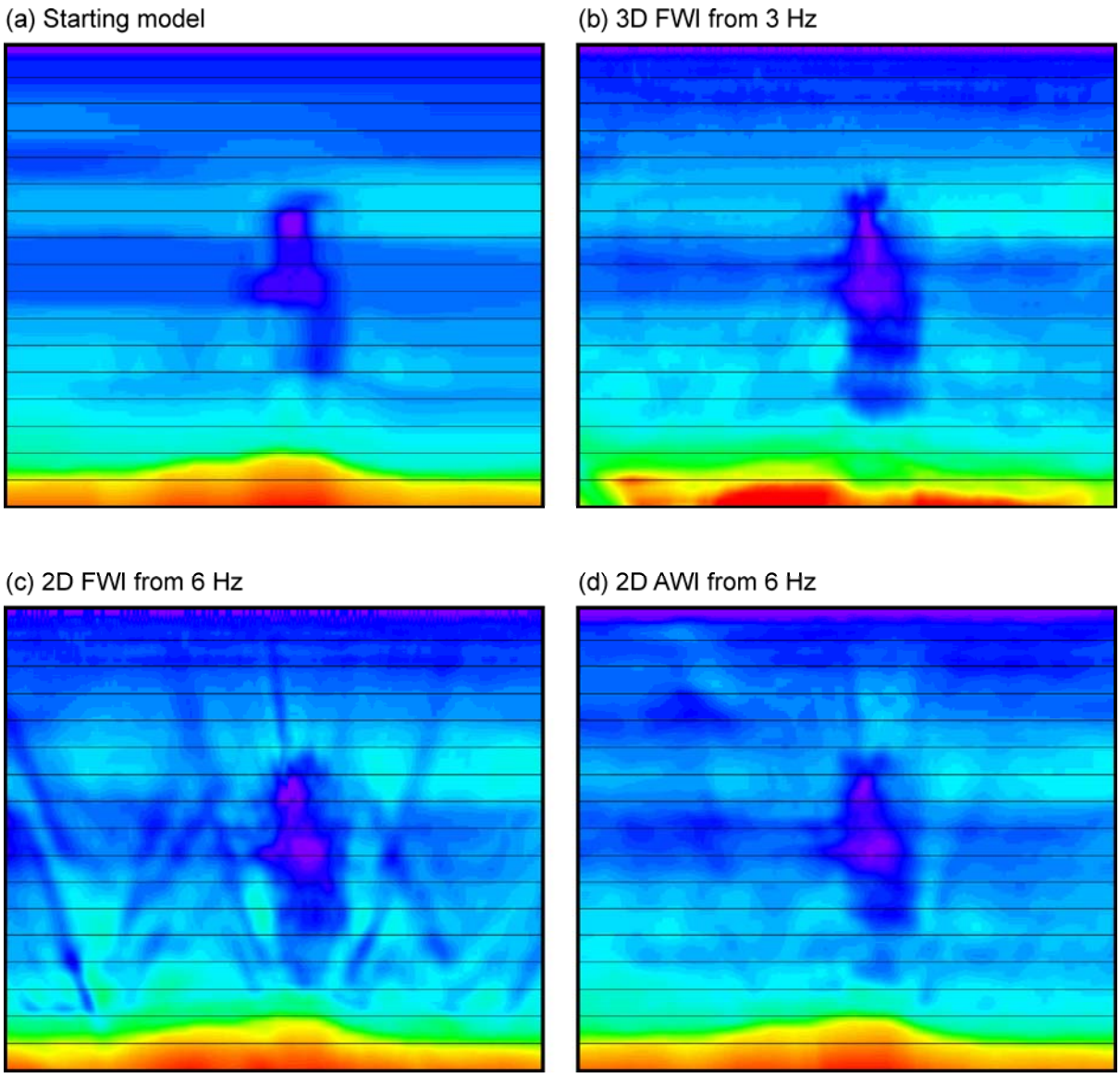


***Figure 1*** *(a) Vertical 2D slice through 3D starting velocity model. (b) Model recovered using 3D conventional FWI starting at 3 Hz. (c) Model recovered by 2D conventional FWI at 6 Hz. (d) Model recovered by 2D adaptive FWI at 6 Hz. Model (c) suffers from cycle skipping while (d) does not.*

The 6 Hz 2D conventional FWI result in Figure 1(c) differs in at least two important aspects from the 3D result at 3 Hz. Firstly, and of the most significance in the present context, the 6 Hz result suffers from the detrimental effects of cycle skipping. This is evidenced by the dipping artefacts that crisscross the section. The 2D result is also inferior as a simple consequence of the 2D geometry. In 3D, the structure is sampled at all azimuths which helps to overcome illumination and other geometric problems, and there are longer offsets available in the 3D dataset. In addition, in a 3D full-azimuth survey, a much greater proportion of the total data volume occupies the longer offsets. These features mean that a 2D result will almost always be inferior to a multi-azimuthal 3D result, especially at depth. These effects are evident within Figure 1(c), but have limited relevance in the present context.

Figure 1(d) shows the model recovered by adaptive FWI. While the figure necessarily shows the illumination and offset limitations inherent in this 2D inversion, the result does not suffer from the effects of cycle skipping that appear in the conventional result at 6 Hz. The geometry of the recovered gas cloud is similar to that recovered in 3D except in its deepest portion, and the model is a better quantitative match to the 3D result. This result confirms that adaptive FWI is immune to the effects of cycle skipping, and that it can be productively applied to field data that do not contain unusually low frequencies. We anticipate that the result that we will obtain for a full-3D adaptive FWI at 6 Hz will match closely the 3D result obtained by conventional FWI when starting at 3 Hz.

**Application to reflection data**

Conventional FWI struggles to recover the long-wavelength macro-velocity model when it is driven predominantly by reflection data without transmitted energy at the target depth. The latter are difficult to acquire for deep targets, and are especially difficult to obtain beneath high-velocity overburden. Transmitted arrivals necessarily have longer travel paths and later arrivals times than do reflections from the same depth. Transmitted arrivals are therefore more prone to cycle skipping and require lower frequencies and a more accurate starting model than do reflected arrivals. Consequently reflection FWI schemes that have increased sensitivity to the macro-velocity model are desirable; adaptive waveform inversion, using weighted Wiener filters, appears to provide such a scheme.

Figure 2 shows conventional and adaptive FWI applied to a simple geometric model that is dominated by reflections rather than refractions except in the shallowest portion of the model. The acquisition geometry consists of a dense spread of fixed receivers across the top of the model; sources are located at every receiver position. Figure 2(a) shows the synthetic model consisting of a water layer, a vertical gradient, and a superimposed checkerboard within which the background velocity varies by ±10%. The starting model, Figure 2(b), contains the correct gradient without the checkerboard; this model is not cycle skipped at the frequencies used here. The modest vertical gradient means that refractions do not penetrate much deeper into the model than the first layer of checkers.

Because the model is not cycle skipped, conventional FWI is able to perform quite well to recover the original model, Figure 2(c). The recovery of the top two layers is almost exact except close to the model edges, and the fit gradually degrades with depth. The deeper portions of the recovered model are all obtained using reflected rather than refracted arrivals. Figure 2(d) shows the gradient of the first iteration generated by conventional FWI; the absolute amplitude is arbitrary, and the gradient is significantly clipped within the red region. It is clear from Figure 2(d) that the inversion is dominated by the effects of shallow refractions, and that the gradient has only weak sensitivity to the reflections.

Figure 2(e) shows the model recovered using adaptive FWI. The results generated by adaptive FWI are superior to those of conventional FWI, especially at depth, but also towards the edges of the model where the effects of refracted energy are reduced. Figure 2(f) shows the gradient for the first iteration. In contrast to conventional FWI, this gradient is influenced by both the shallow refractions, and by deeper reflected energy. This enhanced sensitivity to reflected energy is the reason that Figure 2(e) is superior to Figure 2(c). It comes about because the objective function in equation (1) is only indirectly sensitive to travel-time differences, whereas the objective function in equation (3) is directly sensitive to such time differences; the latter is desirable for effective reflection FWI.

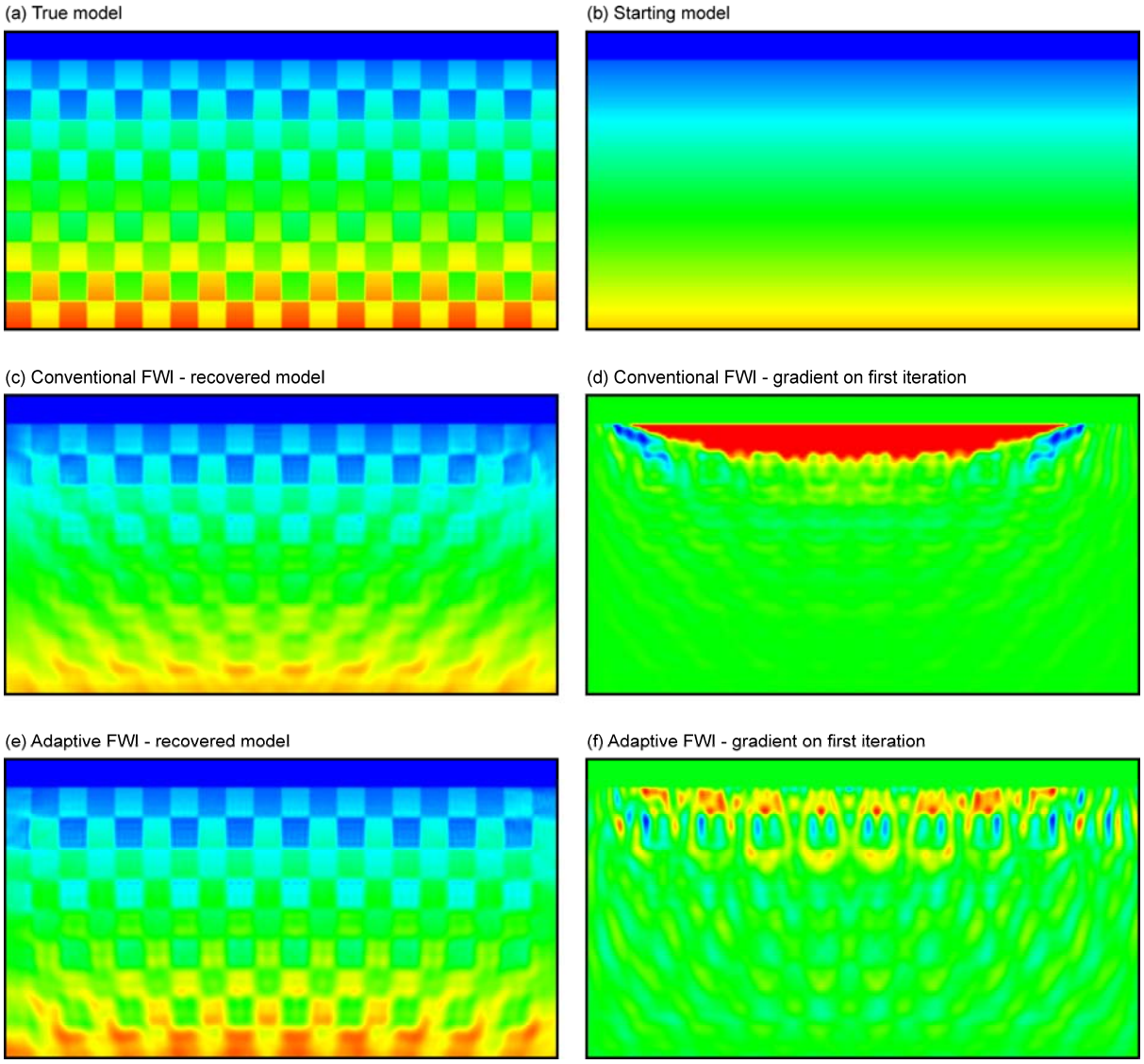


***Figure 2*** *A simple synthetic model demonstrating the superiority of adaptive FWI for reflection data.*

## Conclusions

Adaptive FWI is able to circumvent the requirement for especially low frequencies in field data when applied to datasets that are dominated by refractions. It also appears to have superior performance when applied to datasets that are dominated by reflections, showing enhanced sensitivity to small moveout differences between observed and predicted models. The method readily extends to 3D.

## Acknowledgements

We thank Sub Salt Solutions Ltd for permission to present this paper. The methodology described here is the subject of GB patent application number GB1319095.4.

## References

Warner, M. and Guasch, L. [2014] Adaptive waveform inversion – FWI without cycle skipping: Theory. *EAGE Extended Abstracts*, Amsterdam, 2014.

Warner, M. *et al*. [2013] Anisotropic 3D FWI. *Geophysics*, **78**, R59-R80. doi: 10.1190/GEO2012-0338.1.